

Investigation of two-level defects in injection dependent lifetime spectroscopy

Yan Zhu^{a,*}, Chang Sun^b, Tim Niewelt^{c,d}, Gianluca Coletti^{a,e}, Ziv Hameiri^a

^a School of Photovoltaic and Renewable Energy Engineering, University of New South Wales, Sydney, NSW, 2052, Australia

^b Research School of Electrical, Energy & Materials Engineering, The Australian National University, Canberra, ACT, 2601, Australia

^c Fraunhofer Institute for Solar Energy Systems ISE, Heidenhofstraße 2, 79110, Freiburg, Germany

^d University of Freiburg, Emmy-Noether-Straße 2, 79110, Freiburg, Germany

^e ECN Part of TNO Solar Energy, Westerduinweg 3, 1755, LE Petten, Netherlands



ARTICLE INFO

Keywords:

Defect
Lifetime spectroscopy
Silicon
Boron-oxygen
Light-induced degradation

ABSTRACT

In the majority of studies involving injection dependent lifetime spectroscopy, it is assumed that the investigated defect is a single-level defect following Shockley-Read-Hall recombination statistics. Nevertheless, in real life, two-level defects or multi-level defects are more common than single-level defects. In this study, we first investigated the possible consequences of misinterpreting a two-level defect as two single-level defects. A procedure to properly fit two-level defects in lifetime spectroscopy is subsequently proposed. At the end, we use boron-oxygen related defects as an experimental demonstration. Our experimental results reveal that the recombination statistics of boron-oxygen related defects cannot be explained by the coexistence of two independent single-level defects. A two-level defect parameterization appears to be more suitable.

1. Introduction

Defects in semiconductor reduce the lifetime of photogenerated carriers and therefore, deteriorate the performance of solar cells [1]. Characterization of the electrical properties of defects is essential for identifying them, evaluating their impact on device performance, and eliminating them during the device fabrication processes [2].

Due to its high sensitivity, injection dependent lifetime spectroscopy (IDLS) is widely used for the parameterization of defects' electrical properties [3–6]. By fitting the measured injection dependent lifetime, the solution space of the dominant defect's electrical parameters can be obtained using methods such as Defect Parameter Solution Space (DPSS) [3,7], Defect Parameter Contour Map (DPCM) [8], the Newton-Raphson method [9] and more [10]. The solution space resulting from a single IDLS measurement is ambiguous, i.e., there are an infinite number of solutions of the defect parameters [7]. To reduce this ambiguity it is common to measure injection dependent lifetime at various temperatures (TIDLS) or on samples of various doping concentrations (N_{dop} -IDLS) [3,4,7,11].

In literature, the majority of IDLS analysis focuses on defects following the Shockley-Read-Hall (SRH) [12,13] recombination statistics which assume that the defect has a single energy level within the

bandgap. However, in most of the IDLS-based studies, the fitting of the measured injection dependent lifetime curve by a single SRH defect is not satisfactory [4,7,14–18]. This is usually explained by the existence of a secondary SRH defect in the measured sample [19–23]. This can be a reasonable assumption when the experimental design cannot ensure samples to be limited by just one singular defect. The addition of a secondary SRH defect typically improves the fitting quality to satisfactory precision. However, there is another possible reason for non-satisfactory fitting by a single SRH defect: the measured lifetime is dominated by a multi-level defect instead of a single-level defect [24]. In fact, a recent review paper has demonstrated that many defects feature two or more energy levels in the band gap [25]. Nevertheless, the possibility of multi-level defects has been considered only in a few studies [23,24,26–30]. It is well known that the recombination statistics of a multi-level defect is different from the simple addition of multiple single-level defects [24,25,31]. Therefore, misinterpreting a multi-level defect as multiple single-level defects could result in a significant error in the analysis.

Currently, a thorough investigation of the impact of multi-level defects on IDLS analysis is missing. Furthermore, although in a few studies the injection dependent lifetime has been fitted with a two-level defect model [23,24,26–29], a systematic parameterization procedure for

* Corresponding author.

E-mail address: yan.zhu@unsw.edu.au (Y. Zhu).

multi-level defects has not been developed. In this study, we first use simulation to demonstrate the possible consequences of analyzing a two-level defect as two single-level defects. Then, a procedure to parameterize two-level defects in IDLS is proposed. The findings from the simulation are then applied to a real-life example using boron-oxygen (BO) related defects. In this study we limit ourselves to two-level defects as defects with more than two energy levels in the bandgap require more complicated analysis and will be addressed in a future publication.

2. Simulation study

2.1. Simulation methods

2.1.1. Impact of two-level defects in IDLS

In this study, the impact of two-level defects on an IDLS analysis is evaluated via simulation. First, the injection dependent recombination lifetime of a two-level defect with known defect parameters is simulated. The simulated lifetime is then analyzed assuming it originates from two single-level defects. The defect parameters extracted under this assumption are then compared to the true parameters of the two-level defect.

The recombination lifetime of a two-level defect is simulated using the Sah-Shockley statistics [32]:

$$\tau(\Delta n) = \frac{1 + \left(\frac{\sigma_{n1}\nu_n n_1 + \sigma_{p1}\nu_p p}{\sigma_{p1}\nu_p p_1 + \sigma_{n1}\nu_n n} \right) + \left(\frac{\sigma_{p2}\nu_p p_2 + \sigma_{n2}\nu_n n}{\sigma_{n2}\nu_n n_2 + \sigma_{p2}\nu_p p} \right)}{N_t(n_0 + p_0 + \Delta n) \left[\left(\frac{\sigma_{n1}\sigma_{p1}\nu_n \nu_p}{\sigma_{p1}\nu_p p_1 + \sigma_{n1}\nu_n n} \right) + \left(\frac{\sigma_{n2}\sigma_{p2}\nu_n \nu_p}{\sigma_{n2}\nu_n n_2 + \sigma_{p2}\nu_p p} \right) \right]} \quad (1)$$

where τ is the recombination lifetime of the minority carriers, σ_{nx} (σ_{px}) is the electron (hole) capture cross section where the subscript x denotes the x^{th} defect level ($x = 1$ or 2), ν_n (ν_p) is the thermal velocity of electrons (holes), n_x (p_x) is the electron (hole) density when the Fermi level is at the x^{th} defect energy level E_{tx} , n (p) is the total electron (hole) concentration, N_t is the defect concentration, n_0 (p_0) is the electron (hole) concentration at thermal equilibrium, and Δn is the excess carrier density. In this study, the first energy level refers to the transition energy between the most positively charged state and the middle charge state, whereas the second energy level refers to the transition energy between the middle charge state and the most negatively charged state. For example, for a donor-acceptor type two-level defect, the first energy level is the transition energy between the positive charge state and the neutral state (donor level), while the second energy level is the transition energy between the neutral charge state and the negative charge state (acceptor level).

The simulated injection dependent lifetimes using Eq. (1) is then analyzed assuming two single-level defects, following the SRH recombination statistics [12,13]:

$$\tau(\Delta n) = \frac{(n + n_1)/\sigma_p \nu_p + (p + p_1)/\sigma_n \nu_n}{N_t(n_0 + p_0 + \Delta n)} \quad (2)$$

The parameters of the assumed single-level defect are extracted using a modified DPSS method as suggested in Ref. [33]. First, the lifetime is plotted against a new variable X (for p -type silicon) or Y (for n -type silicon) instead of Δn . X is defined as n/p , whereas Y is defined as p/n [24]. This change of variable transfers the SRH lifetime equation into a linear form (in this case, for a p -type wafer):

$$\tau = \frac{1}{N_t} \left[\left(\frac{1}{\sigma_p \nu_n} + \frac{n_1}{\sigma_p \nu_p p_0} + \frac{p_1}{\sigma_n \nu_n p_0} \right) + X \left(\frac{1}{\sigma_p \nu_p} - \frac{n_1}{\sigma_p \nu_p p_0} + \frac{p_1}{\sigma_n \nu_n p_0} \right) \right] \quad (3)$$

Therefore, the recombination lifetime of a single-level defect is a straight line when plotted against X . A curved $\tau(X)$ plot indicates that more than one defect levels are impacting the lifetime [24]. Assuming that multiple independent single-level defects coexist in the sample, the recombination lifetime can be fitted as the harmonic sum of straight

lines:

$$\begin{aligned} \frac{1}{\tau(X)} &= \frac{1}{\tau_{\text{defect1}}(X)} + \frac{1}{\tau_{\text{defect2}}(X)} + \dots + \frac{1}{\tau_{\text{defect},i}(X)} \\ &= \frac{1}{m_1 X + b_1} + \frac{1}{m_2 X + b_2} + \dots + \frac{1}{m_i X + b_i} \end{aligned} \quad (4)$$

where m_i and b_i are, respectively, the slope and intercept of the linearized recombination lifetime of the i^{th} defect. As can be seen from Eq. (3), the slope and intercept are both a function of the defect parameters (E_t , σ_n and σ_p) and N_t . Conventionally, in IDLS analysis, the defects are parameterized with E_t , ratio of capture cross sections $k \equiv \sigma_n/\sigma_p$, and the electron capture time constant $\tau_n \equiv 1/(\sigma_n \nu_n N_t)$ for p -type silicon or hole capture time constant $\tau_p \equiv 1/(\sigma_p \nu_p N_t)$ for n -type silicon [3].

With m and b for each of the assumed single-level defect determined from fitting the injection dependent lifetime, k and τ_n can be easily calculated as a function of E_t . In this way, the DPSS curves are obtained.

By varying the assumed doping concentration in the simulation and plotting the DPSS curves obtained from the different doping concentrations together, the defect parameters can be extracted from the intersect of the DPSS curves. For a detailed discussion of the physical and analytical background of single level defect analysis, the readers are referred to Refs. [3]. The extracted defect parameters for the assumed single-level defects are then compared to the true defect parameters of the two-level defect in the simulation. As the capture cross sections are always multiplied by N_t in the lifetime equations [Eqs. (1) and (2)], it is not possible to extract the absolute values of capture cross sections from lifetime spectroscopy without the knowledge of N_t [3]. Therefore, in this study, we only compare the values of E_t and k , which are independent of N_t .

It is important to note that the simulation concerns the defect recombination lifetime component only. In practice, the measured lifetime is the effective lifetime of charge carriers, which is impacted by other recombination channels, such as intrinsic recombination and surface recombination. For the analysis of measured lifetime data, it is important to first extract the defect associated recombination lifetime from the measured effective lifetime (see an example below in Section 3.2).

2.1.2. Defect parameterization of two-level defects

The previous section describes the recombination statistics of a two-level defect and the procedure of defect parameterization while misinterpreting it as multiple single-level defects. In this section, a procedure to extract the parameters of a two-level defect from IDLS measurements is presented.

The recombination statistics of a two-level defect involves six independent parameters: E_{t1} , E_{t2} , $N_t \sigma_{n1}$, $N_t \sigma_{p1}$, $N_t \sigma_{n2}$ and $N_t \sigma_{p2}$. Compared to the case of one single-level defect (three parameters), fitting the injection dependent lifetime of a two-level defect is more prone to non-convergency or converging to local minima of the solution space. Furthermore, the conventional DPSS method is not suitable for presenting the solution space of six parameters. We, therefore, propose the following procedure.

We reduce the number of fitting parameters from six to four by fixing the value of E_{t1} and E_{t2} . For a given pair of E_{t1} and E_{t2} , the values of the other four fitting parameters can be obtained from a least-square fitting to minimize the fitting residual. In order to further improve the robustness of the least-square fitting, we repeat the fitting 100 times with randomized initial values for a given pair of E_{t1} and E_{t2} . The other four fit parameters are obtained from the optimal fitting among all these repeated fits. E_{t1} and E_{t2} are then swept across the silicon bandgap and the above fitting procedure is repeated for each combination of E_{t1} and E_{t2} . For each combination, the residual of the fitting, as well as the fitted values for the other four parameters are obtained. These values are then illustrated using two-dimensional maps with E_{t1} and E_{t2} as the two axes. From the map of the fitting residual, the possible solution space of the

two energy levels can be easily identified and the other parameters can be obtained from their corresponding maps (see Fig. 6 below).

2.2. Simulation results and discussion

2.2.1. Impact of two-level defects on conventional IDLS analysis

First, we will illustrate the possible consequences of misinterpreting a two-level defect as two single-level defects in the IDLS analysis. It is obvious that the results depend on the electrical parameters of the two-level defect, as well as the doping and temperature of the sample. Using the simulation method described in Section 2.1.1, we have identified three possible outcomes. Three simulation examples are presented below to illustrate these three cases. In all three simulations, a *p*-type silicon wafer with doping concentration of 10^{16} cm^{-3} at 300 K is used and it is assumed that the effective lifetime of this wafer is completely dominated by a two-level defect with a concentration of 10^{12} cm^{-3} . The electrical parameters of the two-level defect used in these three cases are listed in Table 1. The injection dependent lifetime is calculated in the injection level range between 10^{12} to 10^{17} cm^{-3} .

Case 1. Resulted lifetime cannot be fitted as two single-level defects.

Case 1 is a special case where the recombination lifetime of the two-level defect cannot be fitted as two single-level defects. The calculated injection dependent lifetime of the simulated sample is shown in Fig. 1(a). The corresponded $\tau(X)$ plot is shown in Fig. 1(b). As can be seen, the $\tau(X)$ curve shows a concave shape. As indicated in Eq. (4), in $\tau(X)$ plot the lifetime resulting from two single-level defects should be the harmonic sum of two straight lines, and thus can only be a convex curve. Therefore, a concave $\tau(X)$ plot shown in Fig. 1(b) cannot be explained by the presence of two single-level defects.

This case, therefore, demonstrates that sometimes a single lifetime curve can indicate the presence of a multi-level defect. If a recombination lifetime with a concave $\tau(X)$ curve is measured, it is certain that the lifetime is dominated by a multi-level defect rather than multiple single-level defects. In this case the conventional DPSS method cannot be used to extract meaningful single-level defect parameters.

It should be noted that the shape of the $\tau(X)$ curve is impacted not only by the defect parameters, but also by the temperature and doping concentration. Therefore, Case 1 might occur for a certain two-level defect under certain combinations of temperature and doping, whereas a change of doping or temperature can lead to different cases, as will be described below.

Case 2. Resulted lifetime can be fitted as two single-level defects and correct parameters are obtained.

The calculated $\tau(X)$ curve for the simulated two-level defect of Case 2 is shown as blue dots in Fig. 2. As can be seen, the $\tau(X)$ curve in this case shows a convex shape. As discussed before, in previous IDLS-based investigations, this shape of $\tau(X)$ curve is often explained by two-single level defects. However, this curve was simulated as a multi-level defect using the Sah Shockley formalism. This case illustrates the potential consequence of misinterpreting a two-level defect as two single-level defects.

The calculated lifetime of the two-level defect is fitted as two single-level defects, i.e., as the harmonic sum of two straight lines in $\tau(X)$ plot. The fitting is also shown in Fig. 2. As can be seen, a good fitting quality is

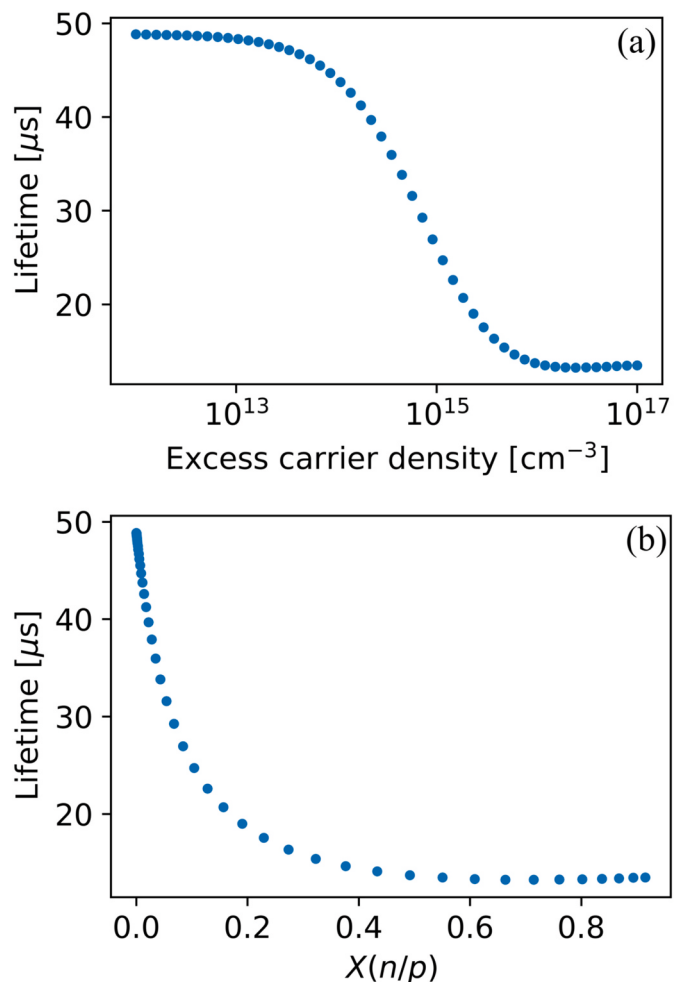


Fig. 1. Calculated injection dependent lifetime of the two-level defect of Case 1 as a function of (a) excess carrier density and (b) the electron and hole concentration ratio. The defect parameters are listed in Table 1 and the sample parameters can be found in the text.

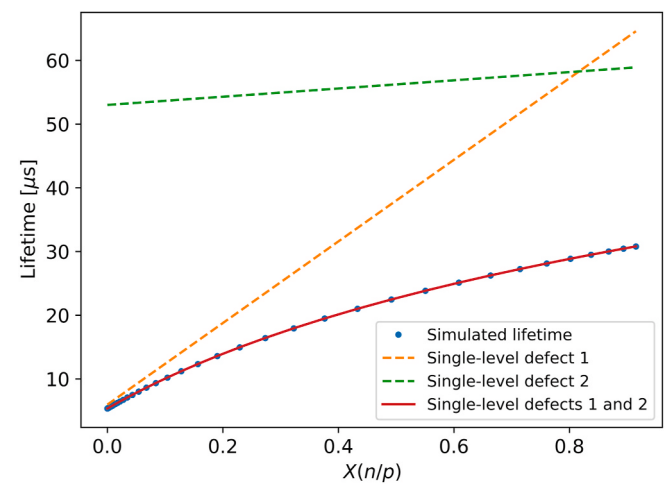


Fig. 2. Calculated injection dependent lifetime of a two-level defect as a function of the electron and hole concentration ratio (dots) for Case 2. The defect parameters are listed in Table 1 and the sample parameters can be found in the text. The lines indicated fitting of the calculated lifetime as two single-level defects.

Table 1

Parameters of the two-level defect used in simulation.

| | Case 1 | Case 2 | Case 3 |
|---------------------------------|------------|------------|---------------------|
| $E_{t1} - E_i$ [eV] | 0.1 | -0.3 | -0.1 |
| σn_1 [cm ²] | 10^{-15} | 10^{-14} | 2×10^{-13} |
| σp_1 [cm ²] | 10^{-15} | 10^{-15} | 10^{-14} |
| $E_{t2} - E_i$ [eV] | -0.1 | 0.1 | -0.5 |
| σn_2 [cm ²] | 10^{-14} | 10^{-15} | 4×10^{-14} |
| σp_2 [cm ²] | 10^{-14} | 10^{-14} | 10^{-13} |

obtained across the entire injection range.

The two single-level defects are then parameterized using the DPSS method and the resulting DPSS- k curves are shown in Fig. 3. The input defect parameters of the simulated two-level defect are indicated by blue dots. As can be seen, for the first level, the DPSS- k curves pass through the correct defect parameters. For the second level, the DPSS- k curve does not pass exactly through the correct defect parameters, however, the deviation is below 0.1% (in terms of k_2 value). The same procedure has been repeated while changing only the doping concentration of the sample from 10^{16} cm^{-3} to $2 \times 10^{15} \text{ cm}^{-3}$ and $2 \times 10^{16} \text{ cm}^{-3}$. For the first level, the DPSS- k curves of all three doping concentrations intersect at the correct defect parameters. For the second level, all three DPSS- k curves are within 0.1% deviation from the true defect parameters. Hence, in this case, although the two-level defect is misinterpreted as two single-level defects, correct defect energy levels and capture cross-section ratios can still be obtained. In this case, the additional energetic transitions between the defect levels and the constraints imposed by the coupled level occupation have only a minor impact on the recombination activity. Such a weak level coupling induces just small effects on the evaluation that could easily be masked by the measurement uncertainty.

Case 3. Resulted lifetime can be fitted as two single-level defects but wrong parameters are obtained.

The calculated $\tau(X)$ plot for the simulated two-level defect in Case 3 is shown in Fig. 4 as blue dots. As is similar to Case 2, the $\tau(X)$ curve shows a convex shape. The lifetime is fitted as two single-level defects and good fitting quality is obtained across the entire injection range, as can be seen in Fig. 4.

Following the same procedure as before, the two single-level defects are parameterized using the DPSS method. However, contrary to the above mentioned Case 2, neither of the DPSS- k curves pass the true defect parameters, indicated by the blue dots in Fig. 5. Even with the variation of doping concentration, none of the DPSS- k curves passes through the correct defect parameters. Thus, in this case,

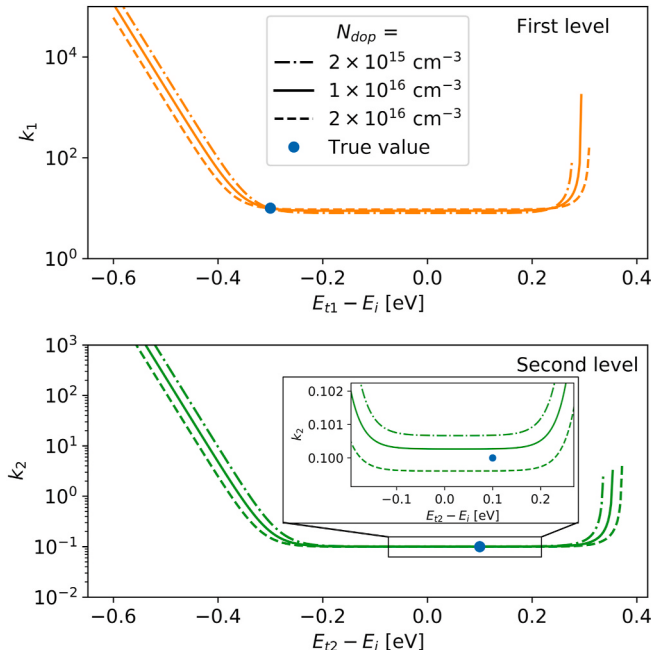


Fig. 3. DPSS- k curves of the two single-level defects used to fit the calculated lifetime in Case 2. The dashed lines and dotted dashed lines indicate results from two other doping concentrations. The true defect parameters of the simulated two-level defect are indicated by blue dots. (For interpretation of the references to colour in this figure legend, the reader is referred to the Web version of this article.)

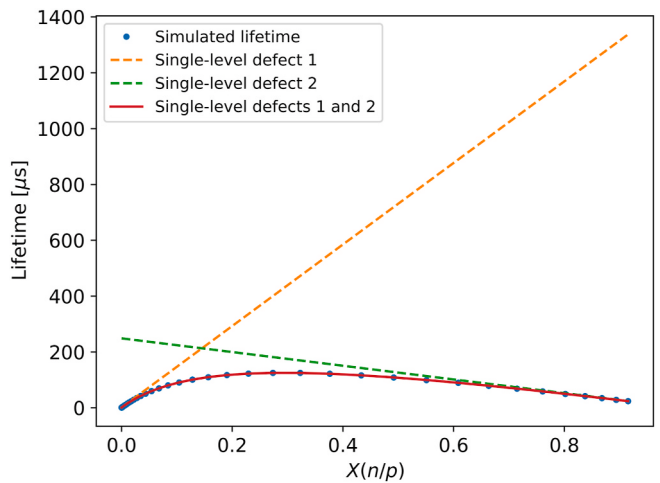


Fig. 4. Calculated injection dependent lifetime of a two-level defect as a function of the electron and hole concentration ratio (dots) for Case 3. The defect parameters are listed in Table 1 and the sample parameters can be found in the text. The lines indicated fitting of the calculated lifetime as two single-level defects.

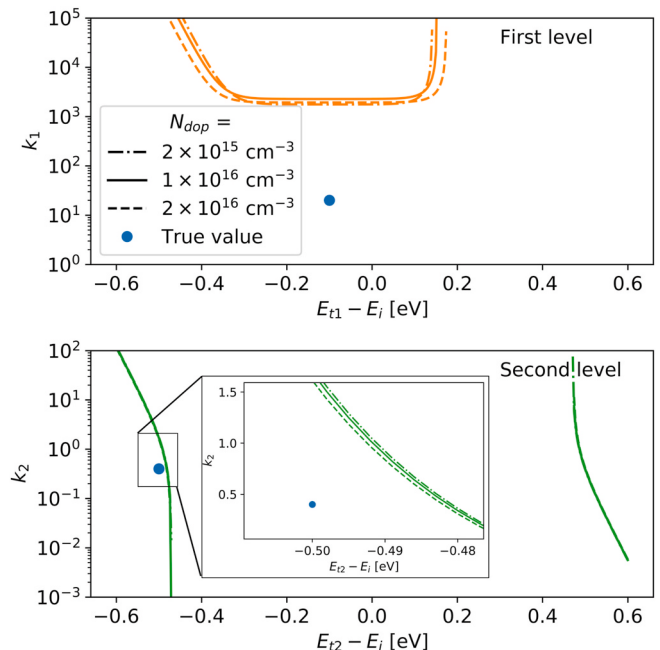


Fig. 5. DPSS- k curves of the two single-level defects used to fit the calculated lifetime in Case 3. The dashed lines and dotted dashed lines indicate results from two other doping concentrations. The true defect parameters of the simulated two-level defect are indicated by blue dots. (For interpretation of the references to colour in this figure legend, the reader is referred to the Web version of this article.)

misinterpreting a two-level defect as two single-level defects results in the wrong defect parameters. This case can be quite dangerous as a good fitting quality of the lifetime curve can still be achieved with the misinterpretation. However, the extracted defect parameters are significantly wrong and of little use for interpretation.

2.2.2. Parameterization of two-level defects in IDLS

In reality, if a $\tau(X)$ with a convex shape is measured, it is difficult to distinguish between Case 2 and Case 3. Therefore, the possibility of two-level defects should be always considered. A procedure to parameterize

the two-level defect in IDLS has been proposed and described in Section 2.1.2. Here we demonstrate this procedure using a set of simulated data. The parameters used in this simulation are the same as for Case 3.

Using the procedure described in Section 2.1.2, we first fit the injection dependent lifetime at 300 K. The resulting map of fitting residual is shown in Fig. 6. As can be seen, there are two large regions in the map showing low fitting residual. For each of the E_{t1} and E_{t2} combinations within these regions, there is a set of $N_t\sigma_{n1}$, $N_t\sigma_{p1}$, $N_t\sigma_{n2}$ and $N_t\sigma_{p2}$ which provides the high quality fit to the injection dependent lifetime. For a given pair of E_{t1} and E_{t2} , the optimal fitting is found to be unique, i.e., there is only one set of $N_t\sigma_{n1}$, $N_t\sigma_{p1}$, $N_t\sigma_{n2}$ and $N_t\sigma_{p2}$ that can achieve the minimal fitting residual when the values of E_{t1} and E_{t2} are fixed. The presented fitting residual map provides a good visualization of the solution space of the defect parameters in this IDLS analysis. The correct combination of the simulated two-level defect is provided as blue dot, which is within the solution space.

From the large regions of low fitting residual, it is clear that the result of defect parameterization from just a single lifetime curve is ambiguous, i.e., there is an infinite number of solutions for the parameters of the two-level defect. This is similar to the IDLS analysis of a single-level defect. In order to reduce the ambiguity, a variation of doping or temperature is needed [3]. Here we use N_{dop} -IDLS for the demonstration. The lifetime of the defect is calculated for both *n*-type and *p*-type silicon with doping concentrations of 10^{16} cm^{-3} and 10^{13} cm^{-3} . The calculated lifetime at different doping conditions are shown as dots in Fig. 7(a). The calculated lifetime curves at these four doping conditions are fitted simultaneously and the resulted fitting residual map is shown in Fig. 7(b). As can be seen, there is one local minimum, which agrees with the input energy level combination of the simulated two-level defect. From this point, $N_t\sigma_{n1}$, $N_t\sigma_{p1}$, $N_t\sigma_{n2}$ and $N_t\sigma_{p2}$ can be extracted and the capture cross section ratios can be easily calculated. However, it should be noted that in the resulting residual map, there is a relatively large region with a low value of fitting residual (below 10^{-4}). In real measurement, when considering measurement uncertainty, it may be challenging to distinguish the minimum point from this large region. In order to have a less ambiguous determination, more variation of the doping condition or temperature is required.

Compared to the DPSS method for single-level defect, the parameterization procedure proposed here for two-level defect is more elaborate. However, as can be seen from the example, the procedure provides a clear visualization of the solution space of the two-level defect's parameters; therefore, it avoids finding only the local minimum or missing solutions in the fitting.

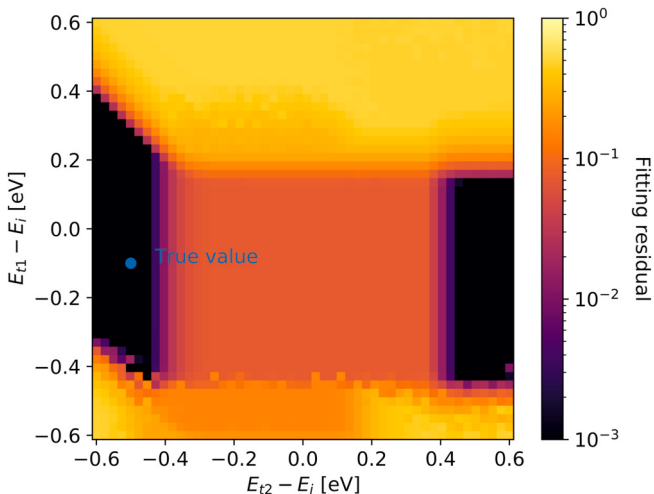


Fig. 6. Fitting residual maps for two-level defect parameterization obtained following the procedure described in Section 2.1.2 for fitting a single set of IDLS data. The correct defect parameters of the two-level defect are also indicated.

3. Demonstration with a real-life case - BO related defects

In Section 2, via simulated data, we illustrated the potential consequences of misinterpreting a two-level defect as two single-level defects in the IDLS analysis. We also proposed a procedure to properly parameterize a two-level defect from IDLS data. In this section, we demonstrate our previous findings and the proposed procedure using measured data of BO-related defect.

It is well known that boron-doped Czochralski (Cz) wafers suffer from bulk degradation when excess carriers are generated (either by illumination or electrical excitation) [14,34–38]. The lifetime of the sample can be recovered upon an annealing at elevated temperature in the dark. However, this recovery is not permanent and degradation can still occur if excess carriers are stimulated in the sample [36,39,40]. If the sample is illuminated at elevated temperature, the sample lifetime can be recovered and stabilized in the high lifetime state. Further generation of excess carriers will then not degrade the lifetime. However, a following dark annealing can destabilize and degrade the lifetime again [34,41].

Although the exact nature of the defect responsible for this degradation is still disputable, it is clear that degradation is related to the boron dopant and oxygen content in the wafer [16,35,39,42–44]. Therefore, we refer to the defect as BO-related defect. It is also well-known that the degradation process involves a fast stage and a slow stage [16,23,27,45,46]. It is still under debate whether the defects responsible for these two stages are two different defects or the same defect [16,23,29,47–50]. However, it has been shown by several research groups that the lifetime at the most degraded state can be described to a satisfactory degree by assuming the presence of two single-level defects or one two-level defect [14–16,23,27]. A study by Niewelt et al. demonstrated that fitting when assuming a two-level defect provides a better fitting quality than assuming two single-level defects [27]. Assuming two-level defect statistics, several groups have suggested its electrical structure to be a negative-U shape defect (the second energy level is above the first energy level) [23,27–29,49].

In this study, we use the BO-related defect as an experimental demonstration assuming it follows the SRH or alternatively the Sah-Shockley statistics. We should note that the exact electrical structure of the defect is still controversial. Recent studies indicate that the capture mechanism for BO-related defect might be trap-assisted Auger capture, and thus it does not follow the SRH or Sah-Shockley recombination statistics [51–55]. We therefore do not aim to determine the exact electrical properties of the BO defect. We chose to discuss this specific defect as an example case where both suggestions of single-level defect superpositions and thorough attempts of two-level defect parameterization exist.

3.1. Experimental method

A boron doped *p*-type Cz wafer ($N_{dop} = 8.5 \times 10^{14} \text{ cm}^{-3}$) and a boron and phosphorus co-doped compensated *n*-type Cz wafer (net $N_{dop} = 2 \times 10^{15} \text{ cm}^{-3}$) are used to demonstrate the proposed method. The interstitial oxygen contents in the *p*-type wafer and compensated *n*-type wafer are measured to be 13.6 ppma and 17.6 ppma, respectively, via Fourier transformed infrared spectroscopy (FTIR) using the ASTM F1188 standard [56]. Both wafers first went through a phosphorus gettering process (785 °C for half an hour) to reduce the concentration of metal impurities. After the gettering process, the samples were first HF (hydrogen fluoride) dipped until hydrophobic, then etched in TMAH (tetramethylammonium hydroxide) solution for 5–6 min to remove the heavily doped layers. The *p*-type wafer was passivated with a 20 nm aluminum oxide (AlO_x) film deposited by atomic layer deposition (ALD) at a deposition temperature of 175 °C. A subsequent forming gas anneal at 425 °C for half an hour was performed to activate the AlO_x surface passivation. The compensated *n*-type wafer was passivated by a 70 nm silicon nitride (SiN_x) film deposited at 300 °C by plasma enhanced

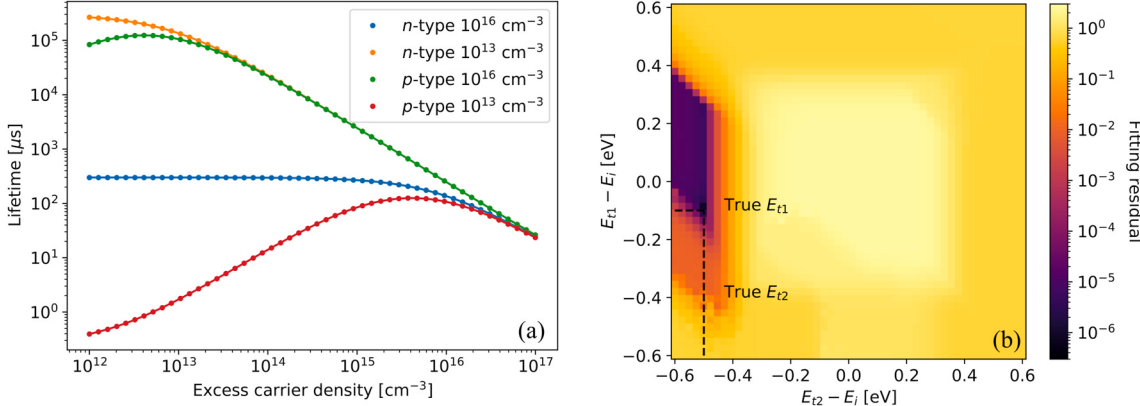


Fig. 7. (a) Calculated injection dependent lifetime of a two-level defect in silicon wafers with four different doping conditions at 300 K. The lines indicate a simultaneous fitting of all the lifetime using the Sah-Shockley statistics. (b) Fitting residual maps for two-level defect parameterization obtained following the procedure described in Section 2.1.2 for fitting simultaneously a set of IDLS at four different doping conditions. (For interpretation of the references to colour in this figure legend, the reader is referred to the Web version of this article.)

chemical vapor deposition (PECVD).

The degradation of the samples was achieved by illuminating the wafers at approximate one sun equivalent illumination using halogen lamps for five days. This ensures that all active defect precursors are activated rendering the samples stable for repeated measurement. The actual sample temperature during the light soaking is around 60 °C (estimated by a thermocouple attached to a dummy sample via Kapton tapes). The deactivation of the defect was achieved by annealing the wafers at 200 °C in the dark for 30 min. The stability of the surface passivation during the degradation and dark annealing is monitored via reference samples of stabilized float-zone (FZ) wafers. The FZ wafers were stabilized by 30 min annealing at 1000 °C in a nitrogen atmosphere [57,58].

The injection dependent lifetime of the samples is measured using a customized lifetime tester featuring temperature dependent lifetime measurement [5], simultaneous photoconductance (PC) [59] and photoluminescence (PL) based lifetime measurements [60]. To minimize the uncertainty in the mobility model of the compensated silicon, the injection dependent lifetime for the compensated *n*-type wafer is obtained by PL based measurements [61].

3.2. Experimental results and discussion

The measured effective lifetime curves of the *p*-type and *n*-type Cz wafers used in this study after dark annealing and light soaking are shown in Fig. 8. For the *p*-type wafer, the lifetime is only measured at 303 K, whereas for the *n*-type wafer the lifetime is measured at 303 K and 343 K. The lifetime of both the *p*-type and *n*-type Cz wafers decreases substantially after light soaking, whereas the lifetime of the FZ control wafers is stable.

To monitor the possibility of association and dissociation of iron-boron (FeB) pairs, the lifetime of the light-soaked samples was also measured after more than 1 h in the dark and immediately after strong flash illumination. No observable change in the measured lifetime has been found, indicating that FeB pairs play a negligible role in these samples.

The defect recombination lifetime is extracted using:

$$\frac{1}{\tau_{\text{defect}}} = \frac{1}{\tau_{\text{LS}}} - \frac{1}{\tau_{\text{DA}}} \quad (5)$$

where τ_{LS} and τ_{DA} are, respectively, the measured effective lifetime of the sample after light soaking and after dark annealing.

The extracted defect lifetime curves of both the *p*-type and *n*-type wafers are shown in Fig. 8 and plotted again in Fig. 9 for a clearer illustration. As can be seen, the lifetime of the *n*-type wafer shows an

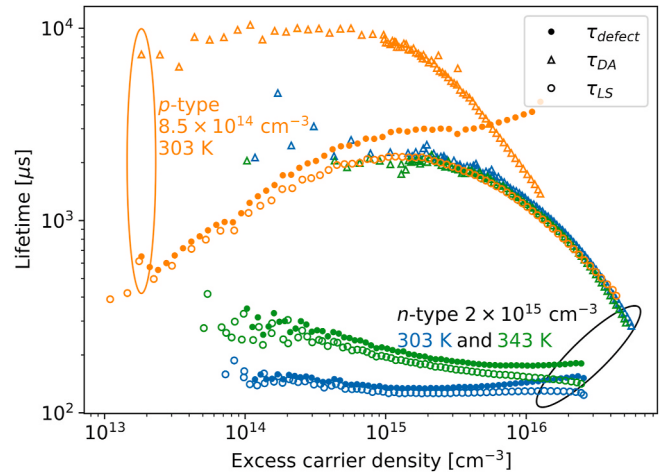


Fig. 8. The measured effective lifetime of the extracted defect recombination lifetime of the *p*-type wafer (at 303 K) and the *n*-type wafer (at 303 K and 343 K) after light soaking and dark annealing. The defect recombination lifetime curves extracted using Eq. (5) are also shown.

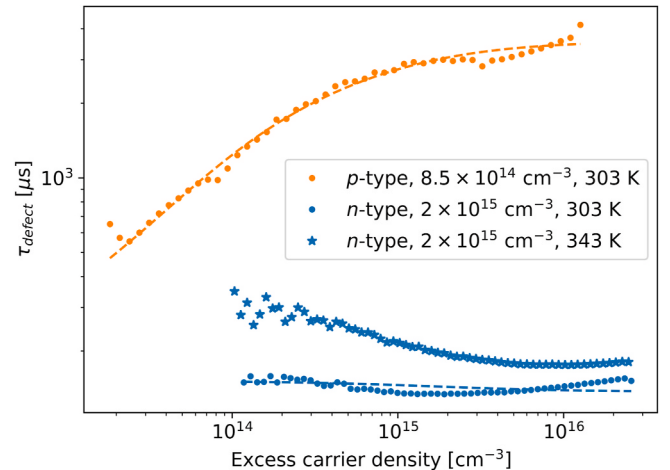


Fig. 9. Extracted defect recombination lifetime of a *p*-type wafer (at 303 K) and an *n*-type wafer (at 303 K and 343 K). The dashed lines indicate fitting of the measured lifetime using the Sah-Shockley statistics.

increase tendency towards lower injection level. This increased tendency is stronger at 343 K than 303 K.

3.2.1. Evidence of BO defect as a two-levels defect

The injection dependent lifetime of the *n*-type wafer is plotted against $Y \equiv p/n$ and shown in Fig. 10. As can be seen, the $\tau(Y)$ at 303 K shows a concave shape. At 343 K, this concave curvature is even stronger.

Comparing Figs. 9 and 10, it can be seen that the concave shape of the $\tau(Y)$ is correlated to the increase of lifetime at low injection levels. It should be noted that this increase of lifetime at low injection cannot be explained by the artefacts induced by depletion region modulation (DRM) [62] or minority carrier trapping [63–66] for the following reasons: (a) the *n*-type wafer is passivated with SiN_x which holds positive fixed charge [67], and there is no heavily doped *p*-type layer near the sample surface; therefore, there is no depletion region presented in the sample; (b) the increase of lifetime at low injection is stronger at higher temperature, this is in contrary to the behavior of minority carrier trapping [68]; and (c) the lifetime is measured by PL which is well known to be hardly impacted by DRM or trapping artefacts [69].

As demonstrated above, this concave shape of $\tau(Y)$ curve cannot be explained by the presence of two single-level defects. Previous works have suggested that the BO-related defect is more likely to be a two-level defect rather than two single-level defects [23,27–29,49]. However, this has been mostly deduced from an improved fitting quality or the *law of parsimony*. The result here provides for the first time direct evidence that the BO-related defects cannot be two single-level defects. It is possible that it is a two-level defect based on the experimental results in this study. However, it should also be noted that recent studies suggest that the BO-related defect might follow the trap-assisted Auger process [51, 55], which leads to recombination statistics different from either the SRH or Sah-Shockley statistics. However, as mentioned previously, the examination of the exact electrical structure of BO-related defects is out of the scope of this study, as we only use it as an experimental demonstration of our simulation findings. Our analysis below is based on the assumption that the BO-related defect is a two-level defect following the Sah-Shockley statistics.

3.2.2. Fitting BO defect with two-level defect

With injection dependent lifetime data of the *p*-type and *n*-type wafer at 303 K, we parameterize the BO-related defect using the procedure proposed above. The lifetime of the *n*-type sample at 343 K is not used, as the temperature dependency of the capture cross section is not known. The resulting fitting residual map is shown in Fig. 11. As can be seen, there are two large regions of low fitting residual. This indicates

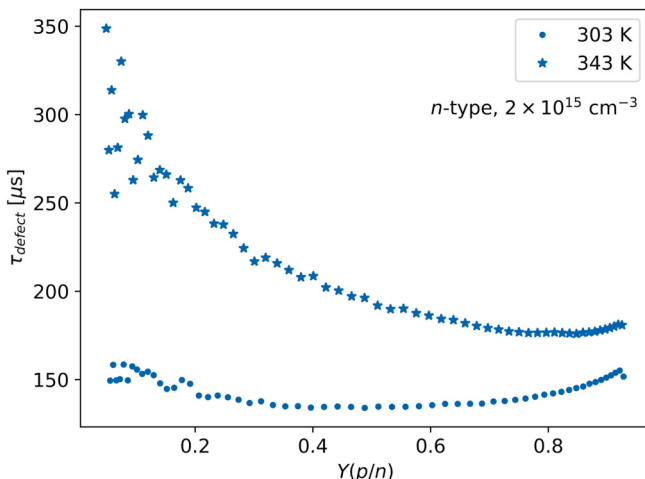


Fig. 10. $\tau(Y)$ plot of the recombination lifetime of the *n*-type wafer at 303 K and 343 K.

that the two wafers used in this study are insufficient to point out the exact energy levels of the defect. A wider doping variation range would be required to reduce this ambiguity of defect parameterization. However, this is again out of the scope of this study. Niewelt et al. recently investigated the BO-related defect as a two-level defect with a wide variation of doping concentration [27]. The energy level combination for BO-related defect extracted by them is marked with a red star in Fig. 11. As can be seen, the energy levels extracted by Niewelt et al. [27] is located in the solution space identified in this study.

3.2.3. Consequence of analyzing BO as two single-level defects

The $\tau(X)$ plot of the *p*-type sample measured at 303 K is shown in Fig. 12(a). As can be seen, it shows a convex shape. This $\tau(X)$ can be fitted assuming two single-level defects. As can be seen from Fig. 12(a), a good fitting quality can be achieved. However, as discussed before, misinterpreting a two-level defect might lead to wrong defect parameterization. The DPSS- k curves of the two single-level defects used to fit the measured $\tau(X)$ data are shown in Fig. 12(b) along with the two-level parameterization by Niewelt et al. [27]. As can be seen, a large deviation between the DPSS- k curves and the reported parameters is observed. Our findings discussed above agree with the identification of the BO-related defect as a multi-level defect. Thus, Fig. 12 demonstrates the consequence of misinterpreting BO-related defect as two single-level defects. This highlights again the importance of considering the possibility of a two-level defect when a convex $\tau(X)$ curve is measured.

4. Conclusions

In this study, the IDLS analysis for the two-level defect was investigated thoroughly. First, the potential consequences of misinterpreting a two-level defect as two single-level defects have been demonstrated via simulation. Depending on the defect parameters, doping concentration and temperature, three different cases can occur: (a) the lifetime of the two-level defect cannot be fitted as two single-level defects; (b) the lifetime of the two-level defect can be fitted as two single-level defects and correct defect parameters can be obtained; and (c) misinterpretation is possible yet the wrong defect parameters are obtained. The study highlights that if the exact electrical structure of the interested defect is unknown it is important not to neglect the possibility of a two-level defect.

Second, a robust procedure to parameterize the two-level defect in IDLS analysis has been proposed and illustrated via simulation. This

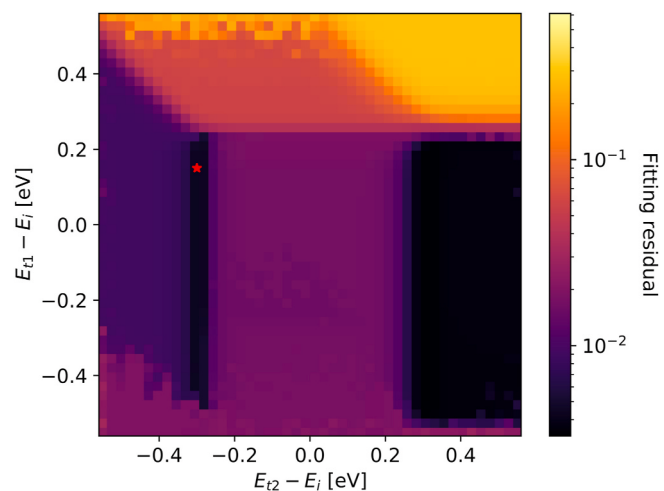


Fig. 11. Fitting residual map for fitting simultaneously the recombination lifetime of the *p*-type and *n*-type samples at 303 K. The red star indicates the defect parameters from Niewelt et al. [27] for the BO related defect. (For interpretation of the references to colour in this figure legend, the reader is referred to the Web version of this article.)

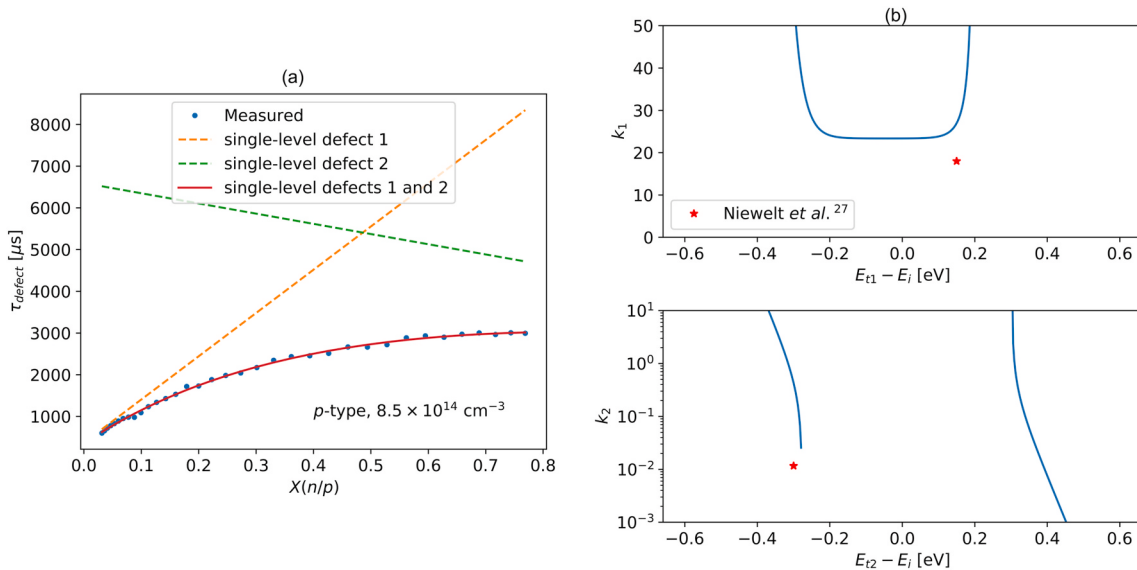


Fig. 12. (a) $\tau(X)$ plot of the recombination lifetime of the p -type wafer. The lines indicate fitting the measured lifetime as two single-level defects. (b) The DPSS- k curves for the two single-level defects. The defect parameters from Niewelt et al. [27] are indicated by the red stars. (For interpretation of the references to colour in this figure legend, the reader is referred to the Web version of this article.)

procedure allows a clear visualization of the solution spaces for a given set of IDLS data.

Finally, we used the BO-related defect as an experimental demonstration of our simulation results. It has been demonstrated that the BO-related defect cannot be explained with two single-level defects. The parameterization of BO-related defect as a two-level defect is also attempted using the proposed procedure. The necessity of using a wider doping range for less ambiguous determination of the defect parameters is highlighted. At the end, the possible error of misinterpreting the BO-related defect as two single-level defects was exhibited, highlighting again the importance of considering two-level defects in IDLS analysis.

Declaration of competing interest

The authors declare that they have no known competing financial interests or personal relationships that could have appeared to influence the work reported in this paper.

CRediT authorship contribution statement

Yan Zhu: Conceptualization, Methodology, Investigation, Writing - original draft. **Chang Sun:** Resources, Writing - review & editing. **Tim Niewelt:** Writing - review & editing. **Gianluca Coletti:** Supervision, Writing - review & editing. **Ziv Hameiri:** Supervision, Writing - review & editing.

Acknowledgement

This work is founded by Australian Government through the Australian Centre for Advanced Photovoltaics (ACAP, project RG200768-G) and the Australian Renewable Energy Agency (ARENA; Project 2017/RND001 and 2017/TND003). C. Sun was also supported by the ARENA ACAP Postdoctoral Research Fellowship. The views expressed herein are not necessarily the views of the Australian Government, and the Australian Government does not accept responsibility for any information or advice contained herein. Part of this work was supported by the German Federal Ministry for Economic Affairs and Energy (BMWi), and by the industry partners within the research cluster LIMES under contract numbers 0324204A and 0324204C.

References

- [1] M.A. Green, Silicon Solar Cells: Advanced Principles and Practice, Centre for Photovoltaic Devices and Systems, University of New South Wales, 1995.
- [2] K. Graff, Metal Impurities in Silicon—Device Fabrication, Springer Science and Business Media, 2013.
- [3] S. Rein, Lifetime Spectroscopy: a Method of Defect Characterization in Silicon for Photovoltaic Applications, Springer Science and Business Media, Berlin, 2006.
- [4] J. Schmidt, Temperature- and injection-dependent lifetime spectroscopy for the characterization of defect centers in semiconductors, *Appl. Phys. Lett.* 82 (2003) 2178–2180, <https://doi.org/10.1063/1.1563830>.
- [5] C. Vargas, Y. Zhu, G. Coletti, C. Chan, D. Payne, M. Jensen, Z. Hameiri, Recombination parameters of lifetime-limiting carrier-induced defects in multicrystalline silicon for solar cells, *Appl. Phys. Lett.* 110 (2017), 092106, <https://doi.org/10.1063/1.4977906>.
- [6] Y. Zhu, F. Rougier, N. Grant, J. Mullins, J.A. De Guzman, J.D. Murphy, V. P. Markevich, G. Coletti, A.R. Peaker, Z. Hameiri, New insights into the thermally activated defects in n-type float-zone silicon, *AIPI Conf. Proc.* (2019) 140014, <https://doi.org/10.1063/1.5123901>.
- [7] S. Rein, T. Rehrl, W. Warta, S.W. Glunz, Lifetime spectroscopy for defect characterization: systematic analysis of the possibilities and restrictions, *J. Appl. Phys.* 91 (2002) 2059–2070, <https://doi.org/10.1063/1.1428095>.
- [8] S. Bernardini, T.U. Naerland, G. Coletti, M.I. Bertoni, Defect parameters contour mapping: a Powerful tool for lifetime spectroscopy data analysis, *Phys. Status Solidi* 255 (2018) 1800082, <https://doi.org/10.1002/pssb.201800082>.
- [9] Y. Zhu, Q.T. Le Gia, M.K. Juhl, G. Coletti, Z. Hameiri, Application of the Newton–Raphson method to lifetime spectroscopy for extraction of defect parameters, *IEEE J. Photovolt.* 7 (2017) 1092–1097, <https://doi.org/10.1109/JPHOTOV.2017.2695666>.
- [10] C. Sun, F.E. Rougier, D. Macdonald, Reassessment of the recombination parameters of chromium in n- and p-type crystalline silicon and chromium-boron pairs in p-type crystalline silicon, *J. Appl. Phys.* 115 (2014) 214907, <https://doi.org/10.1063/1.4881497>.
- [11] M.A. Jensen, Y. Zhu, E.E. Looney, A.E. Morishige, C. Vargas, Z. Hameiri, T. Buonassisi, Assessing the defect responsible for LeTID: temperature- and injection-dependent lifetime spectroscopy, in: 44th IEEE Photovolt. Spec. Conf., 2017, pp. 3290–3294, <https://doi.org/10.1109/PVSC.2017.8366132>.
- [12] W. Shockley, W.T. Read, Statistics of the recombination of holes and electrons, *Phys. Rev.* 87 (1952) 835–842, <https://doi.org/10.1103/PhysRev.87.835>.
- [13] R.N. Hall, Electron-hole recombination in germanium, *Phys. Rev.* 87 (1952), <https://doi.org/10.1103/PhysRev.87.387>, 387–387.
- [14] J. Schmidt, A. Cuevas, Electronic properties of light-induced recombination centers in boron-doped Czochralski silicon, *J. Appl. Phys.* 86 (1999) 3175–3180, <https://doi.org/10.1063/1.371186>.
- [15] S. Rein, S.W. Glunz, Electronic properties of the metastable defect in boron-doped Czochralski silicon: unambiguous determination by advanced lifetime spectroscopy, *Appl. Phys. Lett.* 82 (2003) 1054–1056, <https://doi.org/10.1063/1.1544431>.
- [16] K. Bothe, J. Schmidt, Electronically activated boron-oxygen-related recombination centers in crystalline silicon, *J. Appl. Phys.* 99 (2006), 013701, <https://doi.org/10.1063/1.2140584>.
- [17] L.E. Mundt, M.C. Schubert, J. Schon, B. Michl, T. Niewelt, F. Schindler, W. Warta, Spatially resolved impurity identification via temperature-and injection-dependent

- photoluminescence imaging, *IEEE J. Photovolt.* 5 (2015) 1503–1509, <https://doi.org/10.1109/JPHOTOV.2015.2447837>.
- [18] A.E. Morishige, M.A. Jensen, J. Hofstetter, P.X.T. Yen, C. Wang, B. Lai, D. P. Fenning, T. Buonassisi, *Synchrotron-based investigation of transition-metal getterability in n-type multicrystalline silicon*, *Appl. Phys. Lett.* 108 (2016) 202104.
- [19] W. Warta, Advanced defect and impurity diagnostics in silicon based on carrier lifetime measurements, *Phys. Status Solidi* 203 (2006) 732–746, <https://doi.org/10.1002/pssa.200564510>.
- [20] P. Rosenits, T. Roth, S.W. Glunz, S. Beljakowa, Determining the defect parameters of the deep aluminum-related defect center in silicon, *Appl. Phys. Lett.* 91 (2007) 122109, <https://doi.org/10.1063/1.2789378>.
- [21] S. Diez, S. Rein, T. Roth, S.W. Glunz, Cobalt related defect levels in silicon analyzed by temperature- and injection-dependent lifetime spectroscopy, *J. Appl. Phys.* 101 (2007), 033710, <https://doi.org/10.1063/1.2433743>.
- [22] T. Roth, M. Rüdiger, W. Warta, S.W. Glunz, Electronic properties of titanium in boron-doped silicon analyzed by temperature-dependent photoluminescence and injection-dependent photoconductance lifetime spectroscopy, *J. Appl. Phys.* 104 (2008), 074510, <https://doi.org/10.1063/1.2996252>.
- [23] V. Voronkov, R. Falster, K. Bothe, B. Lim, J. Schmidt, Lifetime-degrading boron-oxygen centres in p-type and n-type compensated silicon, *J. Appl. Phys.* 110 (2011), 063515, <https://doi.org/10.1063/1.3609069>.
- [24] J.D. Murphy, K. Bothe, R. Krain, V. V. Voronkov, R.J. Falster, Parameterisation of injection-dependent lifetime measurements in semiconductors in terms of Shockley-Read-Hall statistics: an application to oxide precipitates in silicon, *J. Appl. Phys.* 111 (2012) 113709, <https://doi.org/10.1063/1.4725475>.
- [25] F.E. Rougieroux, C. Sun, D. Macdonald, Determining the charge states and capture mechanisms of defects in silicon through accurate recombination analyses: a review, *Sol. Energy Mater. Sol. Cells* 187 (2018) 263–272, <https://doi.org/10.1016/j.solmat.2018.07.029>.
- [26] J.D. Murphy, K. Bothe, V.V. Voronkov, R.J. Falster, On the mechanism of recombination at oxide precipitates in silicon, *Appl. Phys. Lett.* 102 (2013), <https://doi.org/10.1063/1.4789858>.
- [27] T. Niewelt, J. Schön, J. Broisch, W. Warta, M. Schubert, Electrical characterization of the slow boron oxygen defect component in Czochralski silicon, *Phys. Status Solidi Rapid Res. Lett.* 9 (2015) 692–696, <https://doi.org/10.1002/pssr.201510357>.
- [28] T. Niewelt, S. Mägfädfessel, M.C. Schubert, Fast in-situ photoluminescence analysis for a recombination parameterization of the fast BO defect component in silicon, *J. Appl. Phys.* 120 (2016), <https://doi.org/10.1063/1.4961423>.
- [29] B. Hallam, M. Kim, M. Abbott, N. Nampalli, T. Nærland, B. Stefani, S. Wenham, Recent insights into boron-oxygen related degradation: evidence of a single defect, *Sol. Energy Mater. Sol. Cells* 173 (2017) 25–32, <https://doi.org/10.1016/j.solmat.2017.06.038>.
- [30] Y. Zhu, G. Coletti, Z. Hameiri, Injection dependent lifetime spectroscopy for two-level defects in silicon, in: 46th IEEE Photovolt. Spec. Conf., 2019, pp. 829–832, <https://doi.org/10.1109/PVSC40753.2019.8981261>. Chicago.
- [31] F.E. Rougieroux, C. Sun, Y. Zhu, D.H. Macdonald, Accurate defect recombination parameters: what are the limitations of current analyses?, in: 7th World Conf. Photovolt. Energy Convers., 2018, pp. 2520–2523, <https://doi.org/10.1109/PVSC.2018.8547585>.
- [32] C. Sah, W. Shockley, Electron-hole recombination statistics in semiconductors through flaws with many charge conditions, *Phys. Rev.* 109 (1958) 1103–1115, <https://doi.org/10.1103/PhysRev.109.1103>.
- [33] A.E. Morishige, M.A. Jensen, D.B. Needelman, K. Nakayashiki, J. Hofstetter, T. A. Li, T. Buonassisi, Lifetime spectroscopy investigation of light-induced degradation in p-type multicrystalline silicon PERC, *IEEE J. Photovolt.* 6 (2016) 1466–1472, <https://doi.org/10.1109/JPHOTOV.2016.2606699>.
- [34] H. Fischer, W. Puschunder, Investigation of photon and thermal induced change in silicon solar cells, in: 10th IEEE Photovolt. Spec. Conf., 1973, pp. 404–411.
- [35] J. Schmidt, K. Bothe, Structure and transformation of the metastable boron- and oxygen-related defect center in crystalline silicon, *Phys. Rev. B* 69 (2004), 024107, <https://doi.org/10.1103/PhysRevB.69.024107>.
- [36] T. Niewelt, J. Schon, W. Warta, S.W. Glunz, M.C. Schubert, Degradation of crystalline silicon due to boron-oxygen defects, *IEEE J. Photovolt.* 7 (2017) 383–398, <https://doi.org/10.1109/JPHOTOV.2016.2614119>.
- [37] D.W. Palmer, K. Bothe, J. Schmidt, Kinetics of the electronically stimulated formation of a boron-oxygen complex in crystalline silicon, *Phys. Rev. B* 76 (2007), 035210, <https://doi.org/10.1103/PhysRevB.76.035210>.
- [38] S.W. Glunz, E. Schäffer, S. Rein, K. Bothe, J. Schmidt, Analysis of the defect activation in CZ-silicon by temperature-dependent bias-induced degradation of solar cells, 3rd World, Conf. Photovolt. Energy Convers. (2003) 919–922.
- [39] J. Schmidt, A.G. Aberle, R. Hezel, Investigation of carrier lifetime instabilities in Cz-grown silicon, in: 26th IEEE Photovolt. Spec. Conf., 1997, pp. 13–18, <https://doi.org/10.1109/pvsc.1997.653914>.
- [40] A. Herguth, G. Hahn, Kinetics of the boron-oxygen related defect in theory and experiment, *J. Appl. Phys.* 108 (2010), <https://doi.org/10.1063/1.3517155>.
- [41] B. Lim, K. Bothe, J. Schmidt, Deactivation of the boron-oxygen recombination center in silicon by illumination at elevated temperature, *Phys. Status Solidi Rapid Res. Lett.* 2 (2008) 93–95, <https://doi.org/10.1002/pssr.200802009>.
- [42] S.W. Glunz, S. Rein, W. Warta, J. Knobloch, W. Wetting, On the degradation of Cz-silicon solar cells, 2nd World, Conf. Photovolt. Energy Convers. (1998) 1343–1346.
- [43] S.W. Glunz, S. Rein, J. Knobloch, W. Wetting, T. Abe, Comparison of boron- and gallium-doped p-type Czochralski silicon for photovoltaic application, *Prog. Photovoltaics Res. Appl.* 7 (1999) 463–469, [https://doi.org/10.1002/\(SICI\)1099-159X\(199911/12\)7:6<463::AID-PIP293>3.0.CO;2-H](https://doi.org/10.1002/(SICI)1099-159X(199911/12)7:6<463::AID-PIP293>3.0.CO;2-H).
- [44] S.Y. Lim, F.E. Rougieroux, D. Macdonald, Boron-oxygen defect imaging in p-type Czochralski silicon, *Appl. Phys. Lett.* 103 (2013), <https://doi.org/10.1063/1.4819096>.
- [45] H. Hashigami, M. Dhamrin, T. Saitoh, Characterization of the initial rapid decay on light-induced carrier lifetime and cell performance degradation of Czochralski-grown silicon, *Jpn. J. Appl. Phys.* 42 (2003) 2564–2568, <https://doi.org/10.1143/JJAP.42.2564>.
- [46] F.E. Rougieroux, B. Lim, J. Schmidt, M. Forster, D. Macdonald, A. Cuevas, Influence of net doping, excess carrier density and annealing on the boron oxygen related defect density in compensated n-type silicon, *J. Appl. Phys.* 110 (2011), 063708, <https://doi.org/10.1063/1.3633492>.
- [47] B. Hallam, M. Abbott, T. Nærland, S. Wenham, Fast and slow lifetime degradation in boron-doped Czochralski silicon described by a single defect, *Phys. Status Solidi Rapid Res. Lett.* 10 (2016) 520–524, <https://doi.org/10.1002/pssr.201600096>.
- [48] M. Kim, M. Abbott, N. Nampalli, S. Wenham, B. Stefani, B. Hallam, Modulating the extent of fast and slow boron-oxygen related degradation in Czochralski silicon by thermal annealing: evidence of a single defect, *J. Appl. Phys.* 121 (2017), 053106, <https://doi.org/10.1063/1.4975685>.
- [49] M. Kim, D. Chen, M. Abbott, N. Nampalli, S. Wenham, B. Stefani, B. Hallam, Impact of interstitial iron on the study of meta-stable B-O defects in Czochralski silicon: further evidence of a single defect, *J. Appl. Phys.* 123 (2018), <https://doi.org/10.1063/1.5000323>.
- [50] J. Schmidt, K. Bothe, V.V. Voronkov, R. Falster, Fast and slow stages of lifetime degradation by boron-oxygen centres in crystalline silicon, *Phys. Status Solidi* (2019) 201900167, <https://doi.org/10.1002/pssb.201900167>.
- [51] M. Vaqueiro-Contreras, V.P. Markevich, J. Coutinho, P. Santos, I.F. Crowe, M. P. Halsall, I. Hawkins, S.B. Lastovskii, L.I. Murin, A.R. Peaker, Identification of the mechanism responsible for the boron oxygen light induced degradation in silicon photovoltaic cells, *J. Appl. Phys.* 125 (2019) 185704, <https://doi.org/10.1063/1.5091759>.
- [52] V.P. Markevich, M. Vaqueiro-Contreras, J.T. De Guzman, J. Coutinho, P. Santos, I. F. Crowe, M.P. Halsall, I. Hawkins, S.B. Lastovskii, L.I. Murin, A.R. Peaker, Boron–oxygen complex responsible for light-induced degradation in silicon photovoltaic cells: a new insight into the problem, *Phys. Status Solidi* 216 (2019) 1900315, <https://doi.org/10.1002/pssb.201900315>.
- [53] P.T. Landsberg, D.J. Robbins, The first 70 semiconductor Auger processes, *Solid State Electron.* 21 (1978) 1289–1294, [https://doi.org/10.1016/0038-1101\(78\)90195-8](https://doi.org/10.1016/0038-1101(78)90195-8).
- [54] P.T. Landsberg, Trap-Auger recombination in silicon of low carrier densities, *Appl. Phys. Lett.* 50 (1987) 745–747, <https://doi.org/10.1063/1.98086>.
- [55] F.E. Rougieroux, C. Sun, M. Juhl, Light-induced-degradation defect independent of the boron concentration: towards unifying admittance spectroscopy, photoluminescence and photoconductance lifetime spectroscopy results, *Sol. Energy Mater. Sol. Cells* 210 (2020) 110481, <https://doi.org/10.1016/j.solmat.2020.110481>.
- [56] ASTM-F1188, Standard test method for interstitial atomic oxygen content of silicon by infrared absorption with short baseline. <https://doi.org/10.1520/F1188-02>, 2003.
- [57] N.E. Grant, V.P. Markevich, J. Mullins, A.R. Peaker, F. Rougieroux, D. Macdonald, J. D. Murphy, Permanent annihilation of thermally activated defects which limit the lifetime of float-zone silicon, *Phys. Status Solidi* 213 (2016) 2844–2849, <https://doi.org/10.1002/pssa.201600360>.
- [58] N.E. Grant, V.P. Markevich, J. Mullins, A.R. Peaker, F. Rougieroux, D. Macdonald, Thermal activation and deactivation of grown-in defects limiting the lifetime of float-zone silicon, *Phys. Status Solidi Rapid Res. Lett.* 10 (2016) 443–447, <https://doi.org/10.1002/pssr.201600080>.
- [59] R.A. Sinton, A. Cuevas, M. Stuckings, Quasi-steady-state photoconductance, a new method for solar cell material and device characterization, in: 25th IEEE Photovolt. Spec. Conf., 1996, pp. 457–460, <https://doi.org/10.1109/PVSC.1996.564042>.
- [60] T. Trupke, R.A. Bardos, Photoluminescence: a surprisingly sensitive lifetime technique, in: 31st IEEE Photovolt. Spec. Conf., 2005, pp. 903–906, <https://doi.org/10.1109/PVSC.2005.1488277>.
- [61] T. Trupke, R.A. Bardos, M.D. Abbott, Self-consistent calibration of photoluminescence and photoconductance lifetime measurements, *Appl. Phys. Lett.* 87 (2005) 184102, <https://doi.org/10.1063/1.2119411>.
- [62] D.H. Neuhaus, P.J. Cousins, A.G. Aberle, Trapping and junction-related perturbations of the effective excess carrier lifetime, 3rd World, Conf. Photovolt. Energy Convers. (2003) 91–94.
- [63] J. Schmidt, K. Bothe, R. Hezel, Oxygen-related minority-carrier trapping centers in p-type Czochralski silicon, *Appl. Phys. Lett.* 80 (2002) 4395–4397, <https://doi.org/10.1063/1.1483908>.
- [64] D. Macdonald, A. Cuevas, Trapping of minority carriers in multicrystalline silicon, *Appl. Phys. Lett.* 74 (1999) 1710–1712, <https://doi.org/10.1063/1.123663>.
- [65] D. Macdonald, R.A. Sinton, A. Cuevas, On the use of a bias-light correction for trapping effects in photoconductance-based lifetime measurements of silicon, *J. Appl. Phys.* 89 (2001) 2772–2778, <https://doi.org/10.1063/1.1346652>.
- [66] Y. Zhu, M.K. Juhl, G. Coletti, Z. Hameiri, Reassessments of minority carrier traps in silicon with photoconductance decay measurements, *IEEE J. Photovolt.* 9 (2019) 652–659, <https://doi.org/10.1109/JPHOTOV.2019.2903584>.

- [67] A.G. Aberle, Overview on SiN surface passivation of crystalline silicon solar cells, *Sol. Energy Mater. Sol. Cells* 65 (2001) 239–248, [https://doi.org/10.1016/S0927-0248\(00\)00099-4](https://doi.org/10.1016/S0927-0248(00)00099-4).
- [68] K.R. McIntosh, B.B. Paudyal, D.H. MacDonald, Generalized procedure to determine the dependence of steady-state photoconductance lifetime on the occupation of multiple defects, *J. Appl. Phys.* 104 (2008) 1–6, <https://doi.org/10.1063/1.2996640>.
- [69] R.A. Bardos, T. Trupke, M.C. Schubert, T. Roth, Trapping artifacts in quasi-steady-state photoluminescence and photoconductance lifetime measurements on silicon wafers, *Appl. Phys. Lett.* 88 (2006) 1–3, <https://doi.org/10.1063/1.2165274>.